International Journal of Thermal Sciences 48 (2009) 1596–1606

Contents lists available at ScienceDirect

International Journal of Thermal Sciences

www.elsevier.com/locate/ijts

Nonsimilar, laminar, steady, electrically-conducting forced convection liquid metal boundary layer flow with induced magnetic field effects ☆

O. Anwar Bég [a,*], A.Y. Bakier [b], V.R. Prasad [c], J. Zueco [d], S.K. Ghosh [e]

[a] Mechanical Engineering Department, Sheaf Building, Sheffield Hallam University, Sheffield, South Yorkshire, S1 1WB, UK
[b] Department of Mathematics, Assiut University, Assiut, Egypt
[c] Department of Mathematics, Madanapalle Institute of Technology and Science, Madanapalle 517325, India
[d] ETS Ingenieros Industriales Campus Muralla del Mar, Departamento de Ingeniería Térmica y Fluidos, Universidad Politécnica de Cartagena, 30203 Cartagena (Murcia), Spain
[e] Department of Mathematics, Narajole Raj College, P.O.-Narajole, Dist.-Midnapore (West), 721 211, West Bengal, India

ARTICLE INFO

Article history:
Received 1 August 2008
Received in revised form 8 December 2008
Accepted 15 December 2008
Available online 20 January 2009

Keywords:
Magnetohydrodynamics
Heat transfer
Boundary layers
Magnetic Prandtl number
Local nonsimilarity method (LNM)
Aligned magnetic field
Astronautics

ABSTRACT

A nonsimilar steady laminar boundary layer model is described for the hydromagnetic convection flow of a Newtonian, electrically-conducting liquid metal past a translating, non-conducting plate with a magnetic field aligned with the plate direction. The non-dimensional boundary layer equations are solved with the *Sparrow–Quack–Boerner local nonsimilarity method* (LNM). An increase in magnetic Prandtl number (Pr_m) is found to strongly enhance wall heat transfer rate ($Nu_x Re_x^{-1/2}$), velocity (f') and induced magnetic field function (g), but exerts negligible influence on the temperature (θ) in the boundary layer. A rise in magnetic force number (β) increases velocity, f', shear stress function, f'', and wall heat transfer gradient, i.e. $Nu_x Re_x^{-1/2}$, but reduces magnetic field function, g and temperature, θ. Increasing ordinary Prandtl number (Pr), decreases temperature, θ, but increases wall heat transfer rate ($Nu_x Re_x^{-1/2}$). An increase in wall to free stream velocity ratio parameter, ζ, increases flow velocity, f', and induced magnetic field gradient, g' for small ξ but reduces g' for larger ξ, and also boosts the wall temperature gradient, $Nu_x Re_x^{-1/2}$. The model has potential applications in astronautical magneto-thermo-aerodynamics, nuclear reactor channel flow control with magnetic fields and MHD (magnetohydrodynamic) energy generators.

1. Introduction

Similarity and nonsimilarity solutions for magnetohydrodynamic (MHD) flows with and without heat transfer have been obtained by various researchers using analytical and numerical methods. Applications of such studies are pertinent in astronautical-re-entry thermo-magneto-aerodynamics [1], MHD energy generator systems [2,3], and magnetohydrodynamic boundary layer-control technologies [4]. Sparrow and Cess [5] presented an early boundary-layer analysis for hydromagnetic natural convection flow. Singh and Cowling [6] used the Pohlhausen approximation to obtain similarity solutions for strong magnetohydrodynamic free convection flow from a vertical heated surface. Jagadeesan [7] studied the influence of magnetic Eckert number with Alfven wave effects on two-dimensional magnetohydrodynamic heat transfer in a parallel plate channel with conducting walls. Gupta [8] used the momentum integral method to obtain similar solutions for magnetohydrodynamic natural convection boundary layer flow from a flat plate. Chawla [9] analyzed the *transient* natural hydromagnetic convection flow from an infinite vertical plate using the Laplace transform technique, showing that magnetic field generates a *wave-dominated* flow pattern and boosts the shear stress at the plate for all time values. Lindauer and Hsu [10] studied transient MHD convection in a channel under short circuit conditions using the method of characteristics, with a step change in the axial pressure gradient or magnetic field. Further excellent studies on MHD convection have been presented by Blum [11] Soundalgekar [12,13], Mazumder [14] who considered a rotating channel, Soundalgekar and Takhar [15] who considered oscillatory, viscous heating and stress work effects and Blum [16] who considered external hydromagnetic boundary layers. Soundalgekar and Ramana Murthy [17] solved the MHD Falkner–Skan and heat transfer equations showing that increasing magnetic parameter boosts skin friction but reduces temperature and an increase in suction reduces skin friction and heat transfer rate. Rao and Rao [18] studied hydromagnetic convection between eccentric rotating disks

☆ Dedicated respectfully to Professor G. Nath (1932–), formerly Professor of Applied Mathematics, Indian Institute of Science, for his tremendous contributions to magnetohydrodynamics and boundary layer research.

* Corresponding author.
E-mail addresses: docoanwarbeg@hotmail.co.uk, O.Beg@shu.ac.uk (O.A. Bég), aybakier@yahoo.com (A.Y. Bakier), rcpmaths@mits.ac.in (V.R. Prasad), joaquin.zueco@upct.es (J. Zueco), g_swapan2002@yahoo.com (S.K. Ghosh).

1290-0729/$ – see front matter
doi:10.1016/j.ijthermalsci.2008.12.007

Nomenclature

x	coordinate along the plate (wall)
y	coordinate transverse to the plate
u	velocity in x-direction
v	velocity in y-direction
H_x	magnetic field component in x-direction
H_y	magnetic field component in y-direction
H_0	applied constant magnetic field
k	thermal conductivity of fluid
u_w	velocity at the wall
u_∞	free stream velocity
T	temperature of the fluid
T_w	temperature at the wall
T_∞	free stream temperature
f	dimensionless stream function
g	dimensionless induced magnetic field
Re_x	local Reynolds number
Pr	Prandtl number
Pr_m	magnetic Prandtl number

Greek symbols

α	thermal conductivity of the fluid
α_1	magnetic diffusivity
β	magnetic force number
ρ	density of the fluid
ν	kinematic viscosity of the fluid
μ_o	magnetic permeability of fluid
φ	stream function
ϕ	induced magnetic field function
ξ	dimensionless streamwise coordinate (nonsimilarity variable parallel to wall)
η	dimensionless transverse coordinate (nonsimilarity variable normal to wall)
ζ	ratio of wall to freestream velocity
θ	dimensionless temperature function

showing that eccentric rotation reduces heat transfer on both disks. Stretching surface hydromagnetic convection with suction was studied by Vajravelu [19]. The supersonic hydromagnetic convection heat transfer from a sphere was studied by Gubin and Shuvalov [20]. Other studies include Soundalgekar and Bhat [21] who considered rarified hydromagnetic convection in a rotating channel, Watanabe [22] who numerically analyzed natural convection hydromagnetic wedge flow, Sacheti et al. [23], Hossain et al. [24] who considered rotating axisymmetric MHD free convection flows, Takhar and Bég [25] who examined computationally the hydromagnetic buoyancy-driven convection in a Darcy–Brinkman–Forchheimer porous medium, Vajravelu and Hadyinicolaou [26] and Bég et al. [27]. Very recently Blum et al. [28] have investigated experimentally hydromagnetic free convection heat transfer from a nonmagnetic cylinder. The above studies have all neglected induced magnetic field effects, i.e. the magnetic field effect has been analyzed in terms of body forces in the momentum equation, rather than as a separate conservation equation. For flows where magnetic Reynolds number is not very small, induced magnetic fields must be considered. Jain and Srinivasan [29] obtained eigenfunction solutions for very small and very high Peclet numbers for thermal entrance region hydromagnetic channel convection flow, showing that an increase in wall electrical conductivity reduces thermal entry lengths. Yu [30] studied steady combined forced and free convection magnetohydrodynamic flow in a vertical plate channel over a range of Hartmann and Rayleigh numbers, showing that magnetic field has a stabilizing effect on the regime. Sloan and Smith [31] investigated the steady laminar hydromagnetic flow in a rectangular pipe between conducting plates, obtaining exact and asymptotic solutions and showing that the induced magnetic field may be matched between the liquid and the plates. Pao and Chang [32] obtained approximate solutions for hydromagnetic boundary layer convection with magnetic field directed in the fluid stream direction, for a magnetic Prandtl number of unity showing that magnetic field increases boundary layer thickness and that steady state solutions are impossible for the case where Alfven wave speed exceeds fluid speed. Megakhed [33] considered the non-stationary hydromagnetic flow from a flat porous plate with induced magnetic field and heat transfer, presenting an exact solution for the flow rate and the induced magnetic field for constant suction and magnetic Prandtl number equal to unity. He showed that such a solution is only tractable when Alfven speed is less than the suction rate. Snyder and Erlasan [34] obtained exact solutions for the average energy dissipation over a duct of arbitrary cross-sectional shape for hydromagnetic channel flow with viscous and Joule heating. Javeri [35] studied Hall and ion slip effects on MHD channel convection, obtaining exact solutions using Kantorowitsch's variational calculus method, for velocity, induced magnetic field and temperature for the case of finely segmented electrodes, fully developed flow and uniform heat flux at channel walls. Mittall et al. [36] computed velocity, magnetic current and efficiency for the MHD generator inlet duct region when the conducting fluid enters the duct with a uniform velocity, showing that the Hall and the ionslip currents generate fluctuations in the current components. Helliwell [37] studied the Couette magnetohydrodynamic compressible flow with thermal radiation, between flat walls of arbitrary electrical conductivity, radiative emissivity and temperature, computing profiles of velocity, induced magnetic field, radiative flux and temperature. Singh and Agarwal [38] presented computational solutions for the velocity and induced magnetic field based on a singular integral equation describing MHD flow through a rectangular pipe with perfectly conducting electrodes. An increase in Hartmann number caused a flattening of the velocity profile and reduced flux through a section. Ezzat and Abd-Elaal [39] used the method of matrix exponentials and also Laplace transforms to study viscoelastic hydromagnetic fluctuating boundary-layer through a porous medium bounded by an infinite non-magnetic vertical plate, presenting distributions of the velocity and the induced magnetic field. Takhar et al. [40] have considered induced magnetic field effects in transient laminar hydromagnetic boundary layer convection along an impulsively-started semi-infinite flat plate with an aligned magnetic field, indicating that a reduction in magnetic Prandtl number will enhance the surface shear stress, surface component of the induced magnetic field and also the surface heat transfer. Koshiba et al. [41] have presented a detailed study of the large-scale pulsed MHD generator system flow including induced magnetic field effects. Gupta et al. [42] have analyzed the hydromagnetic steady shear flow along an electrically insulating porous flat plate, showing that the velocity at a given point increases with increase in either the magnetic field or suction velocity and the induced magnetic field at a given location is reduced with increasing magnetic field. Very recently Chen [43] studied the effects of anisotropic radiative heat transfer on steady magnetohydrodynamic natural convection boundary layer flow from a horizontal plate. However in [43] only the response of Nusselt number to the magnetophysical parameters was discussed. In the present article we therefore assess in much more detail the non-radiative version of the model in [43] dwelling on

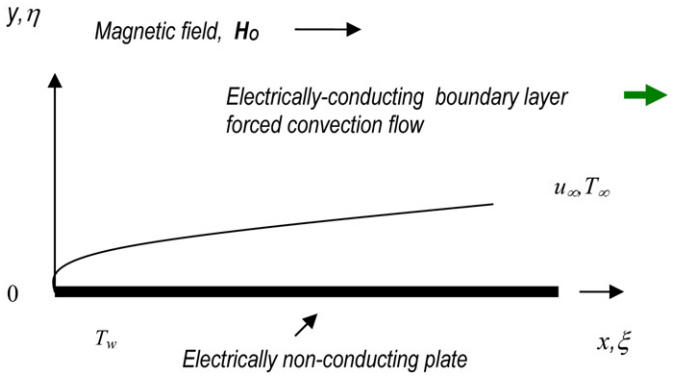

Fig. 1. Physical model and coordinate system.

the variation of velocity field, induced magnetic field and temperature distribution in the boundary-layer. Local nonsimilarity method (LNM) solutions based on the well-tested and extensively validated procedure developed by Sparrow et al. [44] are obtained. Since we are concerned with liquid metal flow we discuss primary and at length the regime for very low Prandtl numbers.

2. Theoretical flow model

Two-dimensional, steady, incompressible, laminar, magnetohydrodynamic thermal convection boundary layer flow of a Newtonian, electrically-conducting, liquid metal (e.g., Mercury) along an electrically non-conducting plate, moving horizontally with constant velocity, u_w, is investigated. The geometry of the flow domain is illustrated in Fig. 1, in which x-coordinate is orientated parallel to the plate with the y-axis normal to this, and the origin located at the leading edge of the plate. A uniform magnetic field, H_o is imposed in the positive x-direction, parallel to the plate and external to the boundary layer. The magnetic Reynolds number is large enough to cause induced magnetic field effects. Following Chen [43], the induced magnetic field vector, $\boldsymbol{H}$, has two components, H_X, H_Y. The normal component of the induced magnetic field, H_y vanishes at the wall with the parallel component, H_X approaching the imposed magnetic field value, H_o, at the edge of the boundary layer. Electrical field, thermal dispersion and viscous and Joule heating effects are neglected. The plate is electrically-non-conducting and maintained at a temperature T_W. The external flow comprises a uniform free stream, u_∞, with a temperature T_∞ ($> T_W$). The governing conservation equations for the boundary-layer flow may be expressed under these simplifications, as follows:

Mass conservation

$$\frac{\partial u}{\partial x}+\frac{\partial v}{\partial y}=0 \tag{1}$$

Magnetic field continuity

$$\frac{\partial H_x}{\partial x}+\frac{\partial H_y}{\partial y}=0 \tag{2}$$

Momentum conservation

$$u\frac{\partial u}{\partial x}+v\frac{\partial u}{\partial y}=\nu\frac{\partial^2 u}{\partial y^2}+\frac{\mu_o}{\rho}\left[H_X\frac{\partial H_X}{\partial y}+H_y\frac{\partial H_X}{\partial y}\right] \tag{3}$$

Induced magnetic field conservation

$$u\frac{\partial H_X}{\partial x}+v\frac{\partial H_X}{\partial y}-H_X\frac{\partial u}{\partial x}-H_y\frac{\partial u}{\partial y}=\alpha_1\frac{\partial^2 H_X}{\partial y^2} \tag{4}$$

Energy (heat) conservation

$$u\frac{\partial T}{\partial x}+v\frac{\partial T}{\partial y}=\alpha\frac{\partial^2 T}{\partial y^2} \tag{5}$$

where all terms are defined in the notation section. The prescribed boundary conditions at the wall (plate) and in the free stream are defined, following Chen [43] as follows:

At $y=0$

$$u=u_\infty;\qquad v=H_y=\frac{\partial H_X}{\partial y}=0;\qquad T=T_w \tag{6a}$$

As $y\to\infty$

$$u\to u_\infty;\qquad H_X\to H_0;\qquad T\to T_\infty \tag{6b}$$

We now introduce the following transformations, in order to normalize the boundary-layer equations:

$$\varphi(x,y)=(\nu u_\infty x)^{1/2}f(x,\eta),\qquad u=\frac{\partial\varphi}{\partial y},\qquad v=-\frac{\partial\varphi}{\partial x}$$

$$\phi(x,y)=\left(\frac{\nu x}{u_\infty}\right)^{1/2}H_0 g(x,\eta),\qquad H_X=\frac{\partial\phi}{\partial y},\qquad H_y=-\frac{\partial\phi}{\partial x}$$

$$\eta=y\left(\frac{u_\infty}{\nu x}\right)^{1/2},\qquad \xi=\beta x Re_x^{-1/2},\qquad \beta=\frac{\nu H_0^2}{u_\infty^2},\qquad Pr=\frac{\rho c_p\nu}{k}$$

$$Pr_m=\frac{\nu}{\alpha_1},\qquad \zeta=\frac{u_w}{u_\infty},\qquad \theta=\frac{T}{T_\infty},\qquad \theta_w=\frac{T_w}{T_\infty},$$

$$Re_x=\frac{u_\infty x}{\nu} \tag{7}$$

where all parameters are defined in the nomenclature. The conservation equations then reduce to the following set of *nonsimilar*, coupled momentum, magnetic and thermal boundary layer equations in a (ξ,η) coordinate system:

$$\frac{\partial^3 f}{\partial\eta^3}+\frac{f}{2}\frac{\partial^2 f}{\partial\eta^2}-\frac{1}{2}\beta g\frac{\partial^2 g}{\partial\eta^2}=\frac{1}{2}\xi\left[\frac{\partial f}{\partial\eta}\frac{\partial^2 f}{\partial\xi\partial\eta}-\frac{\partial^2 f}{\partial\eta^2}\frac{\partial f}{\partial\xi}\right]-\frac{1}{2}\beta\xi\left[\frac{\partial g}{\partial\eta}\frac{\partial^2 g}{\partial\xi\partial\eta}-\frac{\partial^2 g}{\partial\eta^2}\frac{\partial g}{\partial\xi}\right] \tag{8}$$

$$\frac{1}{Pr_m}\frac{\partial^3 g}{\partial\eta^3}+\frac{f}{2}\frac{\partial^2 g}{\partial\eta^2}-\frac{1}{2}\beta g\frac{\partial^2 f}{\partial\eta^2}=\frac{\xi}{2}\left[\frac{\partial f}{\partial\eta}\frac{\partial^2 g}{\partial\xi\partial\eta}-\frac{\partial^2 g}{\partial\eta^2}\frac{\partial f}{\partial\xi}\right]-\frac{\xi}{2}\left[\frac{\partial g}{\partial\eta}\frac{\partial^2 f}{\partial\xi\partial\eta}-\frac{\partial^2 f}{\partial\eta^2}\frac{\partial g}{\partial\xi}\right] \tag{9}$$

$$\frac{1}{Pr}\frac{\partial^2\theta}{\partial\eta^2}+\frac{1}{2}f\frac{\partial\theta}{\partial\eta}=\frac{1}{2}\xi\left[\frac{\partial f}{\partial\eta}\frac{\partial\theta}{\partial\xi}-\frac{\partial f}{\partial\xi}\frac{\partial\theta}{\partial\eta}\right] \tag{10}$$

The dimensionless boundary conditions for the problem now become:

At $\eta=0$

$$f=0;\qquad \frac{\partial f}{\partial\eta}=\zeta;\qquad g=\frac{\partial^2 g}{\partial\eta^2}=0;\qquad \theta=\theta_w \tag{11a}$$

At $\eta\to\infty$

$$\frac{\partial f}{\partial\eta}=1;\qquad \frac{\partial g}{\partial\eta}=1;\qquad \theta=1 \tag{11b}$$

The local Nusselt number may be defined for the boundary-layer regime as:

$$Nu_x Re_x^{-1/2}=\frac{1}{\theta_w-1}\left[-\frac{\partial\theta}{\partial\eta}\right]_{\eta=0} \tag{12}$$

The transformed equations (8) to (10) under conditions (11a), (11b) are to be solved using the LNM method, described in the next section.

3. Numerical solutions with Local Nonsimilarity Method (LNM)

We now obtain approximate solutions to Eqs. (8)–(10) based on the local similarity and local nonsimilarity methods introduced originally by Sparrow et al. [44]. This method has also been used successfully more recently by Gorla et al. [45] who applied it to simulate the mixed thermal convection in a stratified porous medium with dispersion effects. Hassanien et al. [46] have also obtained LNM solutions for the thermal convection boundary layer flow in a non-Darcian regime. For the first level of truncation the ξ derivatives in Eqs. (8)–(10) can be neglected. The governing equations for the first level of the truncation are:

$$\frac{\partial^3 f}{\partial \eta^3} + \frac{1}{2} f \frac{\partial^2 f}{\partial \eta^2} - \frac{1}{2}\beta g \frac{\partial^2 g}{\partial \eta^2} = 0 \tag{13}$$

$$\frac{1}{Pr_m}\frac{\partial^3 g}{\partial \eta^3} + \frac{1}{2} f \frac{\partial^2 g}{\partial \eta^2} - \frac{1}{2}\beta g \frac{\partial^2 f}{\partial \eta^2} = 0 \tag{14}$$

$$\frac{1}{Pr}\frac{\partial^3 \theta}{\partial \eta^2} + \frac{1}{2} f \frac{\partial \theta}{\partial \eta} = 0 \tag{15}$$

with boundary conditions:

At $\eta = 0$

$$f = 0; \qquad \frac{\partial f}{\partial \eta} = \zeta; \qquad g = \frac{\partial^2 g}{\partial \eta^2} = 0; \qquad \theta = \theta_w \tag{16a}$$

At $\eta \to \infty$

$$\frac{\partial f}{\partial \eta} = 1; \qquad \frac{\partial g}{\partial \eta} = 1; \qquad \theta = 1 \tag{16b}$$

For the second level of truncation, we introduce,

$$F = \frac{\partial f}{\partial \xi}, \qquad G = \frac{\partial g}{\partial \xi}, \qquad \Theta = \frac{\partial \theta}{\partial \xi} \tag{17}$$

and restore all of the neglected terms in the first level of truncation. Thus, the governing equations for the second level of truncation are:

$$\frac{\partial^3 f}{\partial \eta^3} + \frac{1}{2} f \frac{\partial^2 f}{\partial \eta^2} - \frac{1}{2}\beta g \frac{\partial^2 g}{\partial \eta^2} = \frac{1}{2}\xi\left[\frac{\partial f}{\partial \eta}\frac{\partial F}{\partial \eta} - \frac{\partial^2 f}{\partial \eta^2}F\right] - \frac{1}{2}\beta\xi\left[\frac{\partial g}{\partial \eta}\frac{\partial G}{\partial \eta} - \frac{\partial^2 g}{\partial \eta^2}G\right] \tag{18}$$

$$\frac{1}{Pr_m}\frac{\partial^3 g}{\partial \eta^3} + \frac{1}{2} f \frac{\partial^2 g}{\partial \eta^2} - \frac{1}{2}\beta g \frac{\partial^2 f}{\partial \eta^2} = \frac{1}{2}\xi\left[\frac{\partial f}{\partial \eta}\frac{\partial G}{\partial \eta} - \frac{\partial^2 g}{\partial \eta^2}F\right] - \frac{1}{2}\xi\left[\frac{\partial g}{\partial \eta}\frac{\partial F}{\partial \eta} - \frac{\partial^2 f}{\partial \eta^2}G\right] \tag{19}$$

$$\frac{1}{Pr}\frac{\partial^2 \theta}{\partial \eta^2} + \frac{1}{2} f \frac{\partial \theta}{\partial \eta} = \frac{1}{2}\xi\left[\frac{\partial f}{\partial \eta}\Theta - F\frac{\partial \theta}{\partial \eta}\right] \tag{20}$$

under the boundary conditions:

At $\eta = 0$

$$f = 0; \qquad \frac{\partial f}{\partial \eta} = \zeta; \qquad g = \frac{\partial^2 g}{\partial \eta^2} = 0; \qquad \theta = \theta_w \tag{21a}$$

At $\eta \to \infty$

$$\frac{\partial f}{\partial \eta} = 1; \qquad \frac{\partial g}{\partial \eta} = 1; \qquad \theta = 1 \tag{21b}$$

The introduction of the three new dependent variables F, G, Θ in the problem requires three additional equations with appropriate boundary conditions. These can be obtained by differentiating Eqs. (18)–(20) with respect to ξ and neglecting the terms $\partial F/\partial \xi$, $\partial G/\partial \xi$ and $\partial \Theta/\partial \xi$. This generates three new equations (omitted for brevity) with corresponding boundary conditions. The coupled non-linear differential equations (13)–(15), (18)–(20) and those generated by differentiation of (18)–(20) with the boundary conditions (16a), (16b), (21a), (21b) are solved computationally using the fourth-order Runge–Kutta method with a shooting technique [44–46]. The step size $\Delta\eta = 0.05$ is used to obtain the numerical solution with five-decimal place accuracy as the criterion of convergence. The LNM method has been extensively validated by the authors in numerous studies [47–50] wherein it has been benchmarked with other finite difference, finite element, asymptotic and network numerical simulation methods. It is extremely accurate and reliable and is therefore not elaborated upon further here.

4. Results and discussion

We utilize the following default data: $Pr_m = 0.1$ (*liquid metal*), $\beta = 0.5$ and $Pr = 0.01$, $\zeta = 0$. The wall temperature is taken as $\theta_w = 1.2$ following Chen [43]. Figs. 2 to 5 illustrate the influence of magnetic Prandtl number (Pr_m) on *the velocity* ($\partial f/\partial \eta = f'$), *induced magnetic field function* (g), *temperature* (θ) *and local Nusselt number function* ($Nu_x Re_x^{-1/2}$) *profiles*. This parameter represents the ratio of the viscous diffusivity to the magnetic diffusivity and is analogous to the ordinary Prandtl number in convection heat transfer, the latter signifying the ratio of the viscous and thermal diffusivities. Pr_m is usually less than or equal to unity and quantifies the relative magnitude of the hydrodynamic and magnetic boundary layer thicknesses. In Fig. 2 we observe that a rise in Pr_m value from 0.1 through 0.3, 0.5, 0.7, 0.9, 1 at a location downstream from the leading edge, i.e. at $\xi = 1$, causes a noticeable rise in the flow velocity, in particular at short distance from the

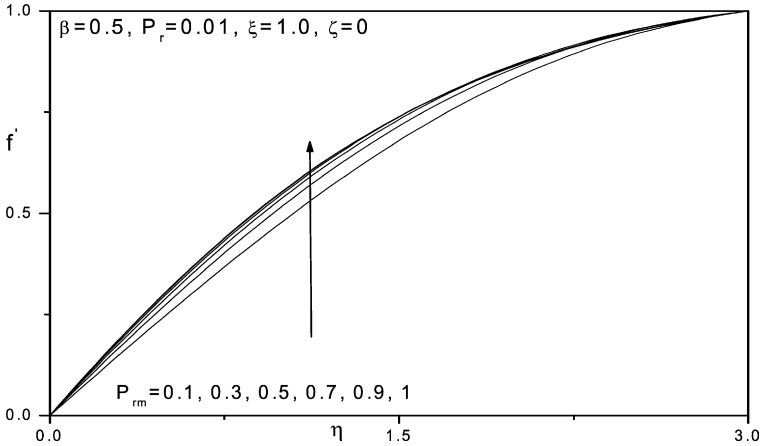

Fig. 2. f' versus η for various Pr_m values.

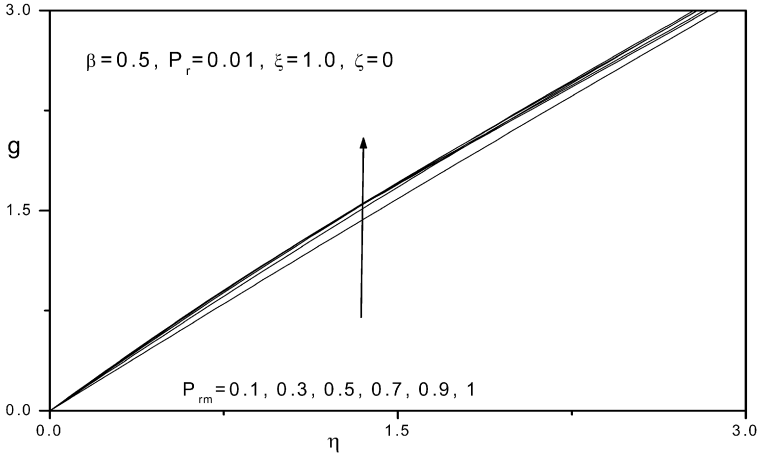

Fig. 3. g versus η for various Pr_m values.

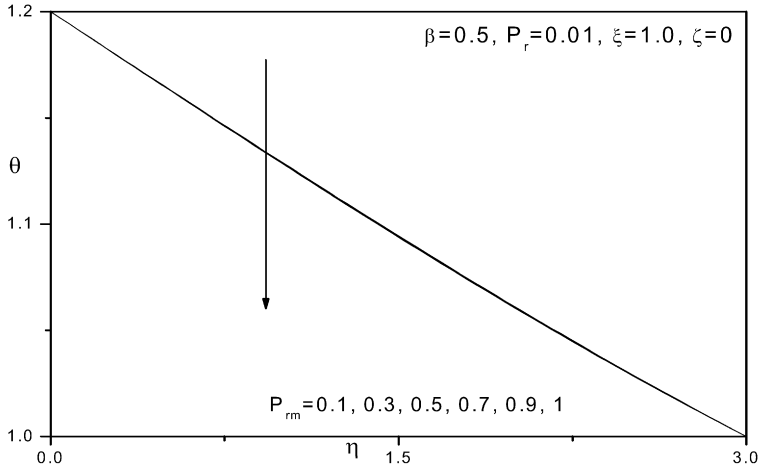

Fig. 4. θ versus η for various Pr_m values.

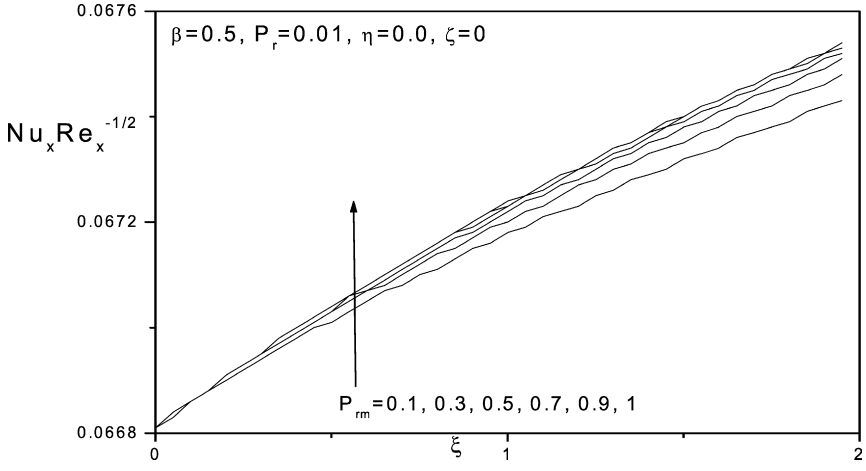

Fig. 5. $Nu_x Re_x^{-1/2}$ versus ξ for various Pr_m values.

plate $\eta \sim 1$. Profiles rise monotonically from the wall to the maximum in the free stream. As such a rise in Pr_m implies a reduction in magnetic diffusivity which *accelerates* the liquid metal boundary layer flow. In Fig. 3 induced magnetic field function, g, is also seen to be slightly enhanced with a rise in Pr_m, i.e. the maximum induced magnetic field corresponds to the maximum Pr_m value of 1, for which the magnetic diffusivity and viscous diffusivity in the boundary layer are equal. Also for $Pr_m = 1$ the magnetic and velocity boundary layers will have an equal thickness. As anticipated temperature, θ, in Fig. 4, is unaffected by a tenfold increase in Pr_m from 0.1, 0.3, 0.5, 0.7, 0.9 to 1, confirming that magnetic diffusivity changing does not exert any tangible influence on the temperature inside the boundary layer regime. However at the wall, a substantial increase in local heat transfer rate, $Nu_x Re_x^{-1/2}$, as shown in Fig. 5, occurs as we progress from the leading edge downstream along the plate, i.e. with increasing ξ, the profiles diverge increas-

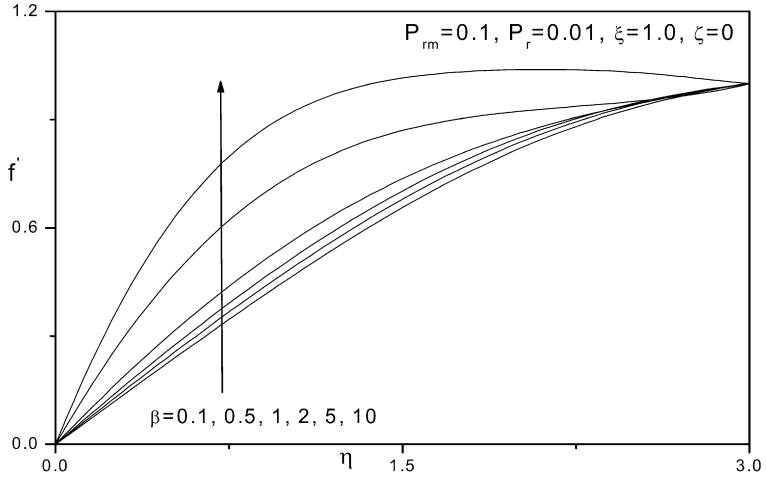

Fig. 6. f' versus η for various β values.

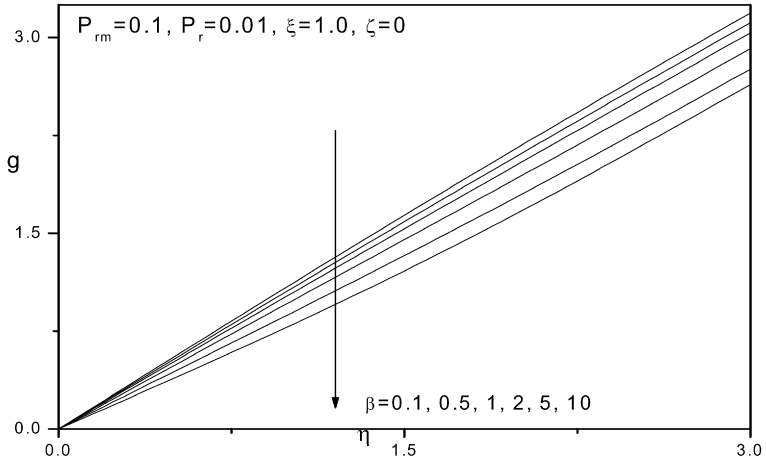

Fig. 7. g versus η for various β values.

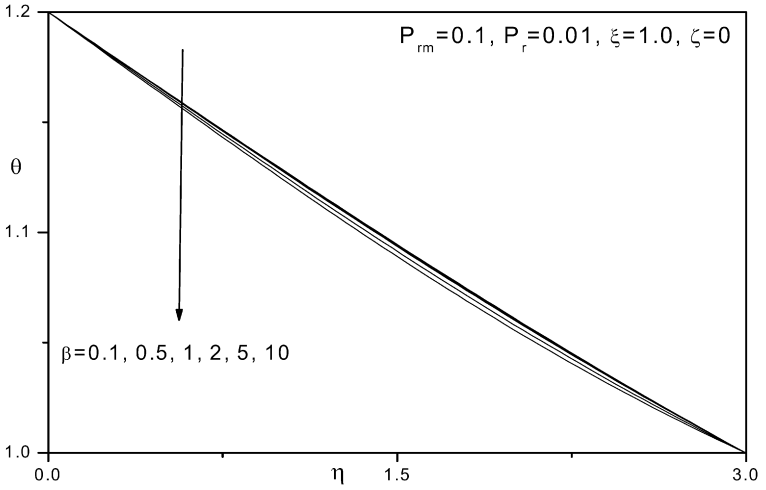

Fig. 8. θ versus η for various β values.

ingly indicating that the maximum wall heat transfer rate for the liquid metal occurs for $Pr_m = 1$ at the maximum distance from the leading edge.

In Figs. 6 to 11 the variation of f', g, θ, f'', g' and $Nu_x Re_x^{-1/2}$ for different values of the magnetic force number, β, are illustrated. $\beta = \nu H_0^2/u_\infty^2$ and as such is proportional to the square of the applied magnetic field, H_0. Since the magnetic field is aligned with the plate, it generates a force transverse to the plate, i.e. in the η-direction. Magnetic field parallel to the plate will therefore accelerate flow along the plate direction leading to an increase in velocity, f', as observed in Fig. 6. For the highest value of β a velocity overshoot is identified in Fig. 6, in consistency with previous studies by Takhar et al. [40]. No such overshoot is encountered for $\beta < 10$. Profiles are seen to be most widely separated again in the

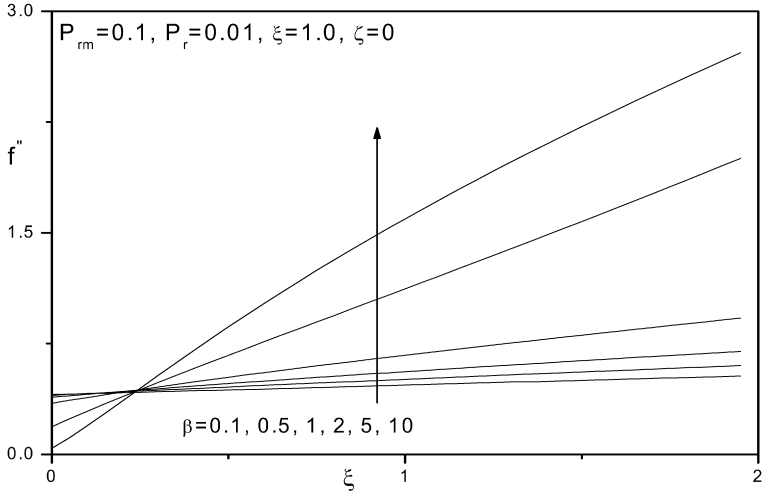

Fig. 9. f'' versus ξ for various β values.

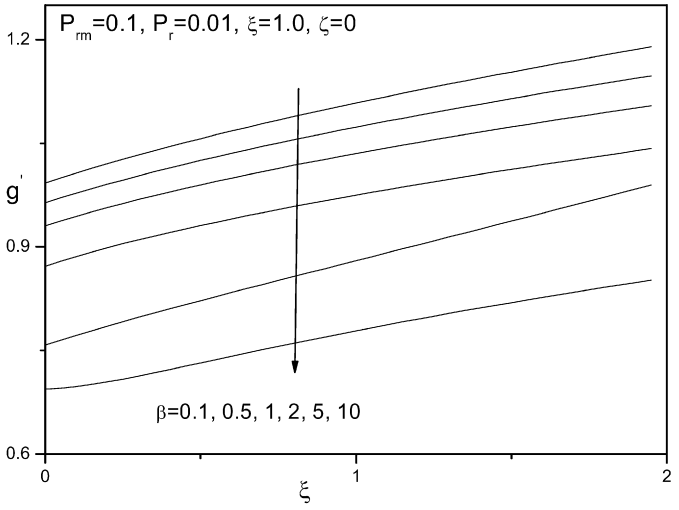

Fig. 10. g' versus ξ for various β values.

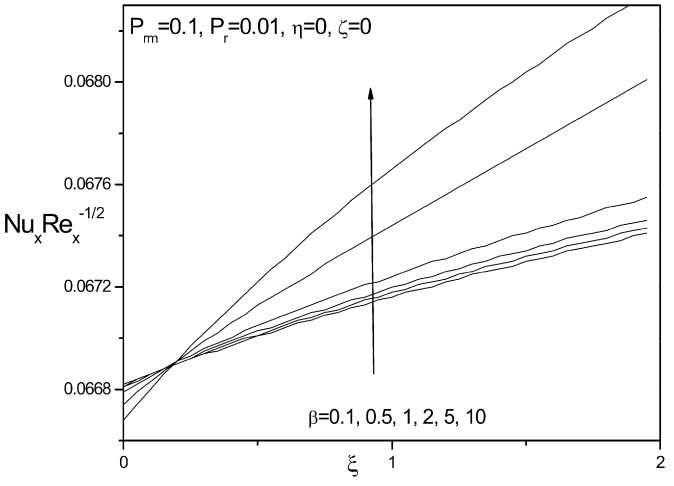

Fig. 11. $Nu_x Re_x^{-1/2}$ versus ξ for various β values.

vicinity of $\eta = 1$, i.e. a short distance transverse to the plate into the boundary layer. Conversely the induced magnetic field, g, is significantly reduced with an increase in magnetic force parameter, β, as depicted in Fig. 7. All profiles are linear ascending to a maximum at the edge of the boundary layer. Similarly temperature is reduced slightly in the boundary layer with an increase in β, since an aligned magnetic field accelerates the flow and reduces thermal energy transfer to the fluid (heat transfer *to* the wall will be increased). The maximum reduction in temperature occurs at intermediate separation from the wall ($\eta \sim 1.5$). Shear stress function (f'') is increased considerably as expected in Fig. 9 since the flow is accelerated along the plate. Initially there is a small reduction close to the leading edge with increasing magnetic force parameter, however for the majority of the distance along the plate ($0.25 < \xi < 2$) f'' profiles are increased considerably and values always maximized at the furthest point from the leading edge. g' values are continuously reduced for all locations along the plate with an increase in β, as indicated by Fig. 10. An increase in applied magnetic field, H_0, therefore suppresses the induced magnetic field, i.e. decreases the magnetic boundary layer thickness. Wall heat transfer gradient, i.e. $Nu_x Re_x^{-1/2} = \frac{1}{\theta_w - 1}[-\frac{\partial \theta}{\partial \eta}]_{\eta=0}$ as depicted in Fig. 11 increases with β values, after a short distance from the leading edge, and the increase is amplified with increasing values of ξ. Aligned magnetic field therefore extracts heat from the fluid to the plate, i.e. the plate is heated whereas the fluid in the boundary layer is cooled, as confirmed by the trend in Fig. 8.

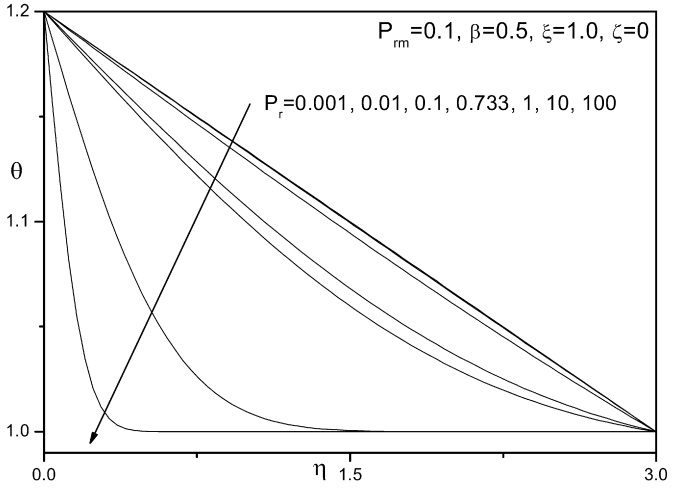

Fig. 12. θ versus η for various Pr values.

In Figs. 12 and 13 the distribution of θ and $Nu_x Re_x^{-1/2}$ are presented for different values of the Prandtl number. A strong decrease in temperature, θ, accompanies a rise in Pr from 0.001 through 0.01, 0.1, 0.733, 1.0, 10.0 to 100, as shown in Fig. 12.

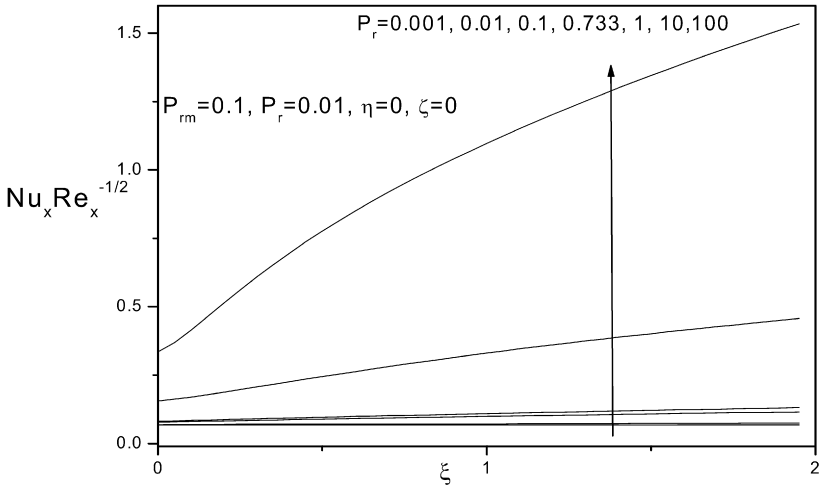

Fig. 13. $Nu_x Re_x^{-1/2}$ versus ξ for various Pr values.

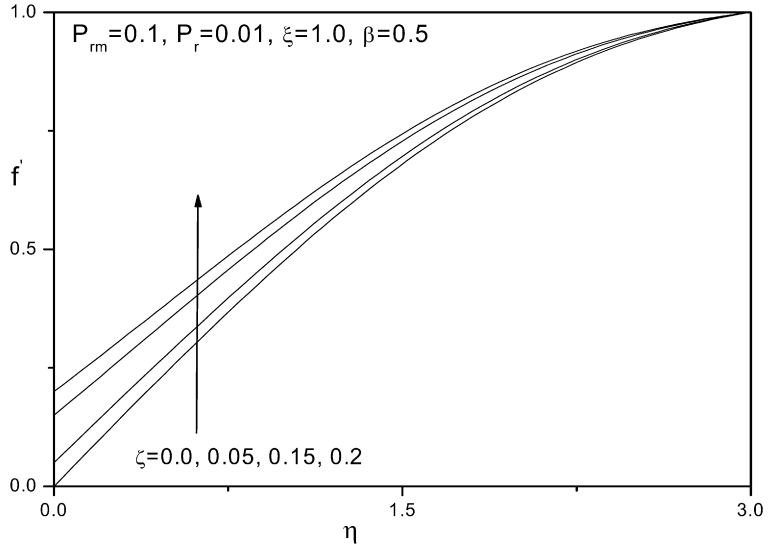

Fig. 14. f' versus η for various ζ values.

Prandtl number defines the ratio of momentum diffusivity to thermal diffusivity. It is directly proportional to the product of dynamic viscosity and specific heat capacity of the fluid and inversely proportional to the thermal conductivity. Smaller Prandtl numbers therefore correspond to a higher thermal conductivity, i.e. liquid metals. With increasing Pr values thermal conductivity will be reduced. For $Pr < 1$ heat diffuses faster than momentum in the boundary layers. For $Pr > 1$ momentum will diffuse faster than heat. Effectively therefore temperatures will be lower with an increase in Prandtl number. At $Pr = 1$ both heat and momentum will diffuse at the same rate and the velocity and thermal boundary layer thicknesses will be approximately the same. It is also worth noting that for liquid metals, e.g., Mercury ($Pr = 0.01, 0.1$) temperature profiles are linear; for higher values of Pr the profiles become increasingly curved. For $Pr = 10$ and 100 (which correspond to electrically-conducting oils) there is an increasing sharpness in reduction of temperature from the wall to a minimal value which is sustained for the remainder of the distance into the boundary layer, transverse to the wall i.e., η-coordinate. In consistency with Fig. 12, wall heat transfer rate ($Nu_x Re_x^{-1/2}$) is considerably boosted in Fig. 13, with an increase in Prandtl number, a pattern which is intensified with increasing distance along the plate, i.e. ξ-coordinate.

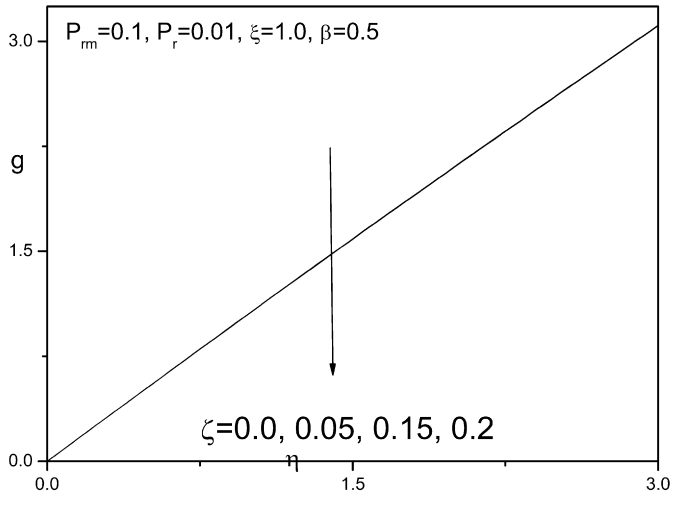

Fig. 15. g versus η for various ζ values.

In Figs. 14 to 19 the effects of the wall to free stream velocity ratio parameter, ζ, on velocity (f'), induced magnetic field function (g), temperature (θ), wall shear stress (f''), wall magnetic

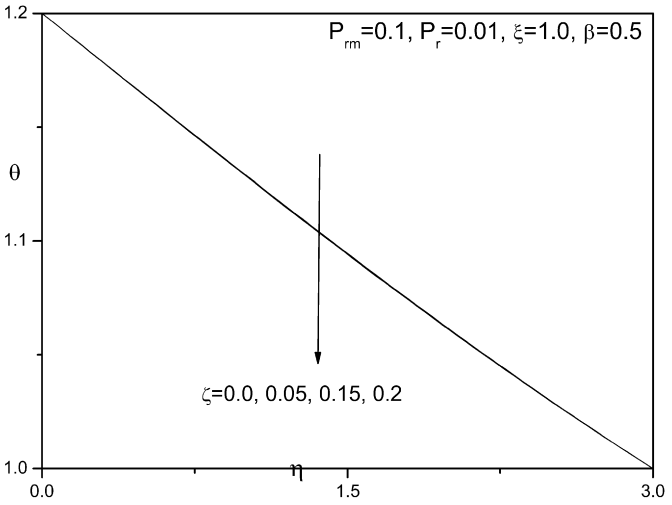

Fig. 16. θ versus η for various ζ values.

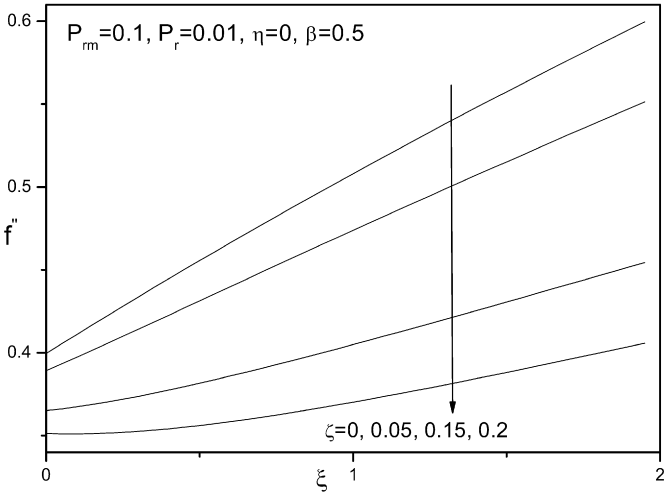

Fig. 17. f'' versus ξ for various ζ values.

field gradient (g') and wall heat transfer rate ($Nu_x Re_x^{-1/2}$). Velocity at the wall is clearly boosted with a rise in ζ and maximized when ζ is a maximum, i.e. 0.2. Profiles as expected rise monotonically with transverse coordinate, η, converging to unity at the edge of the boundary layer. Negligible effects are experienced by the magnetic field function (Fig. 15) and temperature (Fig. 16) since the parameter ζ is associated basically with the hydrodynamic (velocity) boundary layer.

Shear stress function, f'', in Fig. 17, is also substantially decreased for all values of the streamwise coordinate, ξ, with an increase in ζ. Profiles rise consistently from the minimum at the leading edge ($\xi = 0$) to peak at the furthest point along the plate and follow approximately a linear pattern. A slight increase in magnetic field gradient, g' (Fig. 18) accompanies an increase in ζ for low values of ξ. A short distance downstream however there is a switchover in this trend with a clear decrease in g' for greater distances along the plate surface which is maintained for the remainder of the ξ-range. As with shear stress function profiles, the maximum values of g' again arise at the furthest station downstream of the leading edge of the boundary layer. Wall temperature gradient, $Nu_x Re_x^{-1/2}$, is also strongly affected with an increase in wall to free stream velocity ratio parameter, ζ, as shown in Fig. 19. Values are elevated both at the leading edge as ζ increases from 0 through 0.05, 0.15 and 0.2 and climb steadily to their peak magnitudes far downstream along the plate. Heat transfer from the fluid

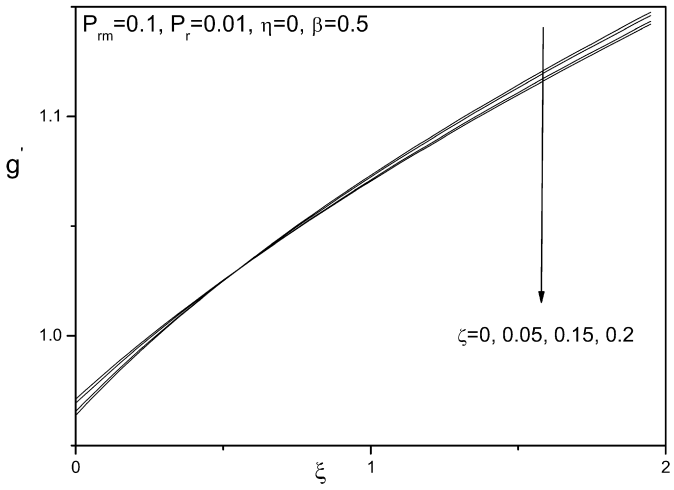

Fig. 18. g' versus ξ for various ζ values.

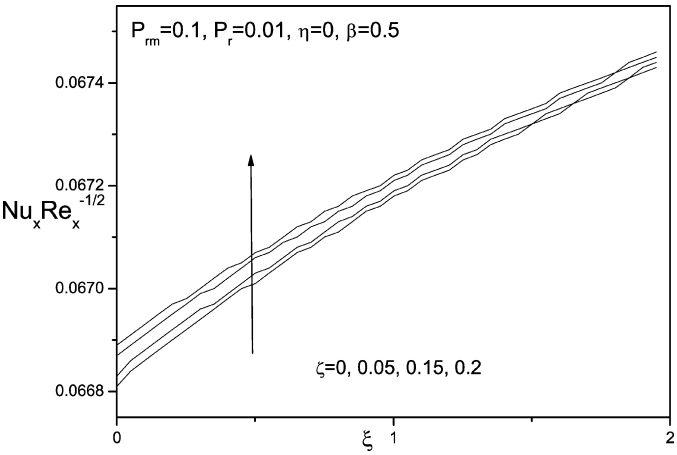

Fig. 19. $Nu_x Re_x^{-1/2}$ versus ξ for various ζ values.

to the plate is therefore enhanced with a rise in free stream velocity.

5. Conclusions

A two-dimensional steady-state laminar magnetohydrodynamic boundary layer thermal convection model for liquid metal flow has been presented including induced magnetic field effects. The robust and rigorously validated Sparrow–Quack–Boerner local nonsimilarity method (LNM) has been implemented to solve the dimensionless velocity, thermal and magnetic boundary layer equations. It has been shown that:

(i) An increase in magnetic Prandtl number, Pr_m, increases velocity (f'), induced magnetic field function (g), and wall heat transfer rate ($Nu_x Re_x^{-1/2}$), but exerts negligible influence on the temperature (θ) in the boundary layer.
(ii) Increasing magnetic force number, β, causes an increase in velocity, f', and causes a velocity overshoot (for high β), decreases induced magnetic field function, g, reduces temperature by a small degree in the boundary layer, boosts shear stress, f'', decreases magnetic field gradient function, g', since an increase in β corresponds to a strong increase in applied magnetic field, H_0, which suppresses the induced magnetic field but accelerates the flow along the plate. Wall heat transfer gradient, i.e. $Nu_x Re_x^{-1/2}$ is also elevated with an increase in β.

(iii) Increasing ordinary Prandtl number, Pr, decreases temperature, θ, in the boundary layer (values are highest for the liquid metal case, $Pr = 0.001$) but enhances wall heat transfer rate ($Nu_x Re_x^{-1/2}$) with increasing streamwise coordinate (ξ).

(iv) An increase in wall to free stream velocity ratio parameter, ζ, increases flow velocity, f', but decreases shear stress function, f'', increases induced magnetic field gradient, g' for small ξ but reduces g' for larger ξ, and *boosts the* wall temperature gradient, $Nu_x Re_x^{-1/2}$. No change in magnetic field function or temperature is however identified with an increase in ζ.

The authors recently extended the current study to incorporate porous media effects [47], again using the Sparrow–Quack–Boerner local nonsimilarity method. Presently the model is being extended to consider the effects of unsteadiness and also variable plate conductivity on boundary-layer characteristics and the results of these investigations will be communicated in the near future.

Acknowledgements

The authors are grateful to both reviewers for their comments which have helped to improve the present article.

References

[1] A. Krishnaswamy, G. Nath, Hypersonic stagnation-point boundary layers with massive blowing in the presence of a magnetic field, Physics Fluids J. 22 (9) (1979) 1631–1638.
[2] M. Sezgin, B.D. Aggarwala, P.D. Ariel, Electrically driven flows in MHD with mixed electromagnetic boundary conditions, Zeitschrift für Angewandte Mathematik und Mechanik (ZAMM) 68 (7) (1988) 267–280.
[3] D. Li, D. Keefer, R. Rhodes, C. Merkle, K. Kolokolnikov, R. Thibodeaux, Analysis of magnetohydrodynamic generator power generation, AIAA J. Propulsion and Power 21 (3) (2005) 424–432.
[4] J.-F. Dietiker, K.A. Hoffman, Boundary layer control in magnetohydrodynamic flows, in: AIAA 40th Aerospace Sciences Meeting and Exhibit, Nevada, USA, 14–17 January, 2002.
[5] E.M. Sparrow, R.D. Cess, Effect of magnetic field on free convection heat transfer, Int. J. Heat Mass Transfer 3 (1961) 267–274.
[6] K.R. Singh, T.G. Cowling, Thermal convection in magnetohydrodynamics I: Boundary layer flow up a hot vertical plate, Quart. J. Mechanics Applied Mathematics 16 (1) (1963) 1–15.
[7] K. Jagadeesan, Heat transfer due to hydromagnetic channel flow with conducting walls, AIAA J. 2 (4) (1964) 756–758.
[8] A.S. Gupta, Hydromagnetic free convection flows from a horizontal plate, AIAA J. 4 (8) (1966) 1439–1444.
[9] S.S. Chawla, Magnetohydrodynamic unsteady free convection, Zeitschrift für Angewandte Mathematik und Mechanik (ZAMM) 47 (8) (1967) 499–508.
[10] C.-J. Hsu, G.C. Lindauer, Unsteady forced-convection MHD heat transfer in a parallel plate channel, AIAA J. 6 (10) (1968) 1973–1979.
[11] E.Y. Blum, Heat and mass transfer in MHD flow past bodies, Magnetohydrodynamics 6 (2) (1970) 69–76.
[12] V.M. Soundalgekar, Free convection effects on steady MHD flow past a vertical porous plate, J. Fluid Mechanics 66 (1974) 541–551.
[13] V.M. Soundalgekar, Free convection effects on the oscillatory flow of an incompressible, electrically conducting, viscous fluid past an infinite, vertical porous plate with constant suction and the transverse magnetic field, Zeitschrift für Angewandte Mathematik und Mechanik (ZAMM) 55 (5) (1975) 257–267.
[14] B.S. Mazumder, Effect of wall conductance on hydromagnetic flow and heat transfer in a rotating channel, Acta Mechanica 28 (1977) 85–99.
[15] V.M. Soundalgekar, H.S. Takhar, MHD oscillatory flow past a semi-infinite plate, AIAA J. 15 (4) (1977) 457–458.
[16] E.Y. Blum, Approximate method for solving problems of free MHD convection near plane and axisymmetric bodies of arbitrary shape, Magnetohydrodynamics 14 (3) (1978) 11–17.
[17] V.M. Soundalgekar, T.V. Ramana Murthy, Heat transfer in MHD flow with pressure gradient, suction and injection, J. Engineering Mathematics 14 (2) (1980) 155–159.
[18] P.R. Rao, A.R. Rao, Heat transfer in MHD flow between eccentric disks rotating at different speeds, Zeitschrift für Angewandte Mathematik und Physik (ZAMP) 34 (4) (1983) 550–555.
[19] K. Vajravelu, Hydromagnetic flow and heat transfer over a continuous, moving, porous flat surface, Acta Mechanica 64 (1986) 179–185.
[20] V.V. Gubin, V.A. Shuvalov, MHD deceleration and heat transfer for a sphere in a supersonic flow of partially ionized gas, J. Applied Mechanics Technical Physics 32 (1) (1991) 12–15.
[21] V.M. Soundalgekar, J.P. Bhat, MHD flow and heat transfer of a rarified gas in a rotating channel between conducting plates, Int. J. Energy Research 16 (6) (1992) 471–480.
[22] T. Watanabe, Magnetohydrodynamic free-convection flow over a wedge in the presence of a transverse magnetic field, Int. Comm. Heat Mass Transfer 20 (1993) 871–881.
[23] N.C. Sacheti, P. Chamdran, A.K. Singh, An exact solution for unsteady magnetohydrodynamic free convection flow with constant heat flux, Int. Comm. Heat Mass Transfer 21 (1994) 131–142.
[24] M.A. Hossain, S.K. Das, I. Pop, MHD free convection flow near rotating axisymmetric round-nosed bodies, Magnetohydrodynamics 32 (1) (1996) 63–67.
[25] H.S. Takhar, O.A. Bég, Effects of transverse magnetic field, Prandtl number and Reynolds number on non-Darcy mixed convective flow of an incompressible viscous fluid past a porous vertical flat plate in a saturated porous medium, Int. J. Energy Research 21 (1997) 87–100.
[26] K. Vajravelu, A. Hadyinicolaou, Convective heat transfer in an electrically-conducting fluid at a stretching surface with uniform stream velocity, Int. J. Engineering Science 35 (1997) 1273–1285.
[27] O.A. Bég, H.S. Takhar, G. Nath, A.J. Chamkha, Mathematical Modeling of hydromagnetic convection from a rotating sphere with impulsive motion and buoyancy effects, Non-Linear Analysis: Modeling and Control J. 11 (3) (2006) 227–245.
[28] E.Y. Blum, A. Mezulis, G. Kronkalns, Magnetoconvective heat transfer from a cylinder under the influence of a nonuniform magnetic field, J. Physics: Condensed Matter 20 (2008) 204–210.
[29] M.K. Jain, J. Srinivasan, Hydromagnetic heat transfer in the thermal entrance region of a channel with electrically-conducting walls, AIAA J. 2 (1) (1964) 1886–1892.
[30] C.P. Yu, Combined forced and free convection channel flows in magnetohydrodynamics, AIAA J. 3 (6) (1965) 1184–1186.
[31] D.M. Sloan, P. Smith, Magnetohydrodynamic flow in a rectangular pipe between conducting plates, Zeitschrift für Angewandte Mathematik und Mechanik (ZAMM) 46 (7) (1966) 439–443.
[32] H.P. Pao, C.C. Chang, Magnetohydrodynamic boundary layer between parallel streams of different magnetic fields and temperatures, AIAA J. 4 (8) (1966) 1313–1320.
[33] A.A. Megakhed, Effect of induced magnetic field and heat transfer on nonstationary magnetohydrodynamic flow around a porous plate, Magnetohydrodynamics 10 (1) (1974) 48–52.
[34] W.T. Snyder, A.H. Erlasan, Energy dissipation in MHD duct flow, AIAA J. 7 (1) (1969) 150–151.
[35] V. Javeri, Influence of Hall effect and ion slip on velocity and temperature fields in an MHD channel, Heat Mass Transfer 7 (4) (1974) 226–235.
[36] M.L. Mittall, G.H. Masapati, V.K. Rohatgi, Performance of magnetohydrodynamic generator in the inlet region, Int. J. Energy Research 3 (2) (1979) 189–199.
[37] J.B. Helliwell, Radiative magnetogasdynamic Couette flow with variable parameters, Zeitschrift für Angewandte Mathematik und Physik (ZAMP) 30 (5) (1979) 811–824.
[38] B. Bani Singh, P.K. Agarwal, Numerical solution of a singular integral equation appearing in magnetohydrodynamics, Zeitschrift für Angewandte Mathematik und Physik (ZAMP) 35 (6) (1984) 760–770.
[39] M.A. Ezzat, M.Z. Abd-Elaal, State space approach to viscoelastic fluid flow of hydromagnetic fluctuating boundary-layer through a porous medium, Zeitschrift für Angewandte Mathematik und Mechanik (ZAMM) 77 (3) (1997) 197–207.
[40] H.S. Takhar, A.J. Chamkha, G. Nath, Unsteady flow and heat transfer on a semi-infinite flat plate with an aligned magnetic field, Int. J. Engineering Science 37 (13) (1999) 1723–1736.
[41] Y. Koshiba, T. Matsushita, M. Ishikawa, Influence of induced magnetic field on large-scale pulsed MHD generator, in: AIAA 33rd Plasmadynamics and Lasers Conference, Maui, Hawaii, May 20–23, 2002.
[42] A.S. Gupta, J.C. Misra, M. Reza, Magnetohydrodynamic shear flow along a flat plate with uniform suction or blowing, Zeitschrift für Angewandte Mathematik und Physik (ZAMP) 56 (6) (2005) 1030–1047.
[43] T.-M. Chen, Radiation effects on magnetohydrodynamic free convection flow, Technical Note, AIAA J. Thermophysics Heat Transfer 22 (1) (2008) 125–128.
[44] E.M. Sparrow, H. Quack, J. Boerner, Local non-similarity boundary layer solutions, AIAA J. 8 (1970) 1936–1942.
[45] R.S.R. Gorla, A.Y. Bakier, L. Byrd, Effects of thermal dispersion and stratification on combined convection on a vertical surface embedded in a porous medium, Transport in Porous Media 25 (3) (1996) 275–282.
[46] I.A. Hassanien, A.Y. Bakier, R.S.R. Gorla, Effects of thermal dispersion and stratification on non-Darcy mixed convection from a vertical plate in a porous medium, Heat and Mass Transfer 34 (2–3) (1998) 209–212.
[47] O.A. Bég, T.-B. Chang, J. Zueco, R. Bhargava, Numerical analysis of nonsimilar super-Alfven hydromagnetic forced convection flow in porous media with induced magnetic field effects, J. Plasma Physics (2008), submitted for publication.

[48] O.A. Bég, H.S. Takhar, A.Y. Bakier, V.R. Prasad, J. Zueco, Numerical analysis of natural convective magnetohydrodynamic heat and mass transfer from isothermal sphere to non-Darcy regime with Soret/Dufour and transpiration effects, Applied Math. Modelling (2008), submitted for publication.
[49] O.A. Bég, T.A. Bég, A.Y. Bakier, V.R. Prasad, Chemically-reacting mixed convective heat and mass transfer along inclined and vertical plates with Soret and Dufour effects: local nonsimilarity numerical solutions, International J. Applied Mathematics and Mechanics (2008), in press.
[50] O.A. Bég, A.Y. Bakier, V.R. Prasad, Laminar mixed convection heat and mass transfer in boundary layer flow along an inclined plate with Soret/Dufour effects, Mathematical and Computer Modelling J. (2008), submitted for publication.